We are IntechOpen,
the world's leading publisher of
Open Access books
Built by scientists, for scientists

4,800
Open access books available

122,000
International authors and editors

135M
Downloads

Our authors are among the

154
Countries delivered to

TOP 1%
most cited scientists

12.2%
Contributors from top 500 universities

Interested in publishing with us?
Contact book.department@intechopen.com

Numbers displayed above are based on latest data collected.
For more information visit www.intechopen.com

Effect of Precipitation on Cryogenic Toughness of N-Containing Austenitic Stainless Steels After Aging

Maribel L. Saucedo-Muñoz and
Victor M. Lopez-Hirata

Additional information is available at the end of the chapter

Abstract

This chapter shows the effect of intergranular precipitation on the cryogenic toughness of N-containing austenitic stainless steels in comparison to that for 316-type austenitic stainless steels. First part of the chapter deals with the thermodynamic stability and growth kinetics of the precipitated phases in the austenite matrix based on Thermo-Calc software. To continue, the experimental evolution of precipitation for N-containing steels is compared to that of 316-type steel and the difference between them are explained based on the Thermo-Calc PRISMA-calculated results. Finally, the effect of intergranular precipitation on the cryogenic fracture toughness is also analyzed using Charpy V-Notch impact test results. The fracture mode is also related to the precipitation characteristics.

Keywords: N-containing austenitic stainless steel, precipitation, aging, toughness

1. Introduction

Austenitic stainless steels are used to construct different equipments with good corrosion resistance in most of the principal industries, for instance, the chemical, petroleum, and nuclear power industries. These structural materials are iron alloys, which contain a minimum of about 11% chromium. This content of chromium enables the formation of a passive film, which is self-protecting in different environments [1].

Nowadays, there are more than 200 different alloys, which can be recognized as belonging to the stainless steel group, and each year new ones and modifications of existing ones appear. In some stainless steels, the chromium content now approaches 30%, and many other elements are added to provide specific properties or ease of fabrication. For example, nickel,

nitrogen, and molybdenum are added for corrosion resistance; carbon, molybdenum, nitrogen, titanium, aluminum, and copper for strength; sulfur and selenium for machinability; and nickel for formability and toughness.

Nitrogen is an alloying element, which has been used in iron-based alloys since the beginning of last century and it has been studied during the last three decades. However, nitrogen steels are so far not widely employed. The reason for this is related to the old customer skepticism in relation to nitrogen is an element, which causes brittleness in the steels.

In the case of austenitic stainless steels, the main motivating force in the development of nitrogen-containing steels is the much higher yield and tensile strengths reached, in comparison with the conventionally processed austenitic stainless steels without losing its toughness. Nitrogen-containing stainless steels present yield and tensile 200–350% higher than those of the AISI 300 series steels. Moreover, the yield strength can be increased above 2 GPa by cold deformation process because of its work hardening potential. It is also important to note that, in contrast to carbon-containing austenitic steels, nitrogen-containing austenitic stainless steels keep a high fracture toughness at low temperatures, higher than 200 Pa m$^{-1/2}$ [2].

The higher mechanical properties of nitrogen-containing austenitic stainless steels have made its application very attractive in the power-generation industry, shipbuilding, railways, cryogenic process, chemical equipment, pressure vessels, and nuclear industries.

This kind of steels contains supersaturated nitrogen levels, and it is susceptible to intergranular precipitation of chromium nitride (Cr_2N) as same as the AISI 300 series stainless steels are prone to the precipitation of chromium carbide ($Cr_{23}C_6$). If the precipitation of chromium took place, the stainless steel is susceptible to sensitization, which may cause intergranular corrosion and intergranular stress corrosion cracking [2]. Nevertheless, the chromium depletion due to the nitride precipitation for nitrogen-containing steels has been reported [3, 4] to be lower than that of carbide precipitation for the AISI 300 series steels, which causes a lower degree of sensitization in the former steel.

In addition, the intergranular precipitation and coarsening of chromium-rich precipitates have been observed to cause a decrease in the toughness of austenitic stainless steels. This type of microstructural deterioration has been named as "thermal aging". It has been reported that the precipitation is very complex, being able to involve more than 20 different precipitated phases [5]. This thermal aging may also occur in the heat-affected zones during the welding of these steels causing the decrease in toughness especially at cryogenic temperatures.

Therefore, the purpose of this chapter is to describe the kinetic behavior of precipitation during the isothermal aging of N-containing austenitic steels and its effect on cryogenic toughness, as well as its comparison with 300 series austenitic stainless steels.

2. Thermodynamics and kinetics of precipitation

This section shows the thermodynamic stability of solid phases in three austenitic stainless steels whose chemical composition is shown in **Table 1**. The first chemical composition

corresponds to an AISI 316L steel and the other two, designated as A1 and A2 steels, correspond to N-containing steels. All these steels can be used for cryogenic applications since they possess good fracture toughness at temperatures as low as liquid nitrogen temperature. The highest interstitial solute contents, Ni and Cr contents are for the A2 steel. A1 steel has the highest content of Mn and the lowest contents of Cr and Ni.

The thermodynamic analysis of these steels was carried out using the commercial software, Thermo-Calc [6]. **Figure 1(a–c)** shows the equilibrium pseudobinary Fe-C at temperature lower than 1000°C and low carbon contents for each of the three steels. In the case of 316 steels, **Figure 1(a)**, a solvus line is observed, which separates the austenite region, FCC_A1, from the austenite and $M_{23}C_6$ carbide, FCC_A1 + $M_{23}C_6$. $M_{23}C_6$ carbide is the more general designation of $Cr_{23}C_6$, which is the main carbide precipitated in austenitic Cr-Ni steels. It has a fcc crystalline structure. As temperature decreases, several phases are formed such as σ (SIGMA) phase, χ (CHI) phase, and ferrite (BCC_A2). σ phase has a tetragonal unit cell with a composition FeCr. χ (CHI) phase is a bcc intermetallic phase with a typical composition of $Fe_{36}Cr_{12}Mo_{10}$ [1, 2]. In the case of A1 steel, **Figure 1(b)**, there is no phase region corresponding only to the austenite phase, FCC_A1, but a phase mixture of austenite and M_2N, HCP_A#2, which usually substitute $M_{23}C_6$ in N-containing austenitic stainless steel, and it has a close packed hexagonal unit cell. This nitride is also designated as Cr_2N. As the temperature decreases, $M_{23}C_6$ becomes stable. A further decrease in temperature promotes additionally the formation of the σ phase. The A2 steel has a similar behavior for phase formation than that showed in the diagram of the A1 steel, **Figure 1(c)**.

On the other hand, **Figure 2(a–c)** shows the expected phases during aging at temperatures of 500–1000°C for these three steels. In the case of 316 steel, the precipitation of σ phase and $M_{23}C_6$ is favored in the austenite matrix. In contrast for the N-containing steels, the precipitation of M_2N, HCP_A#2, and $M_{23}C_6$ in the austenite matrix is more likely to occur during aging at these temperatures. Besides, the precipitation of the σ phase is also possible for these two steels. A remarkable point of these diagrams is that the bcc ferrite (BCC_A2) phase is clearly present in the 316 and A2 steels, but it is absent in the case of A1 steel. This is attributable to the high content of Mn, an austenite-former. This fact suggests the possible formation of delta ferrite during the solidification of 316 and A2 steels, which is associated with a brittle behavior [1]. The precipitation behavior for the steels is shown in the Time-Temperature-Precipitation (TTP) diagram for these steels, as shown in **Figure 3(a–c)**. These diagrams were calculated using Thermo-Calc PRISMA [7] for grain boundary precipitation considering the following parameters: grain size of 100 μm, interfacial energy for the interfaces $\gamma/M_{23}C_6$, $\gamma//M_2N$, and γ/σ of 0.15, 0.22, and 0.28 J/m², respectively [8]. Aging process was analyzed for times up to

Steel	C	N	Mn	Si	Cr	Ni	Mo
316	0.03	–	1.4	0.35	16.8	10.4	2.0
A1	0.05	0.25	21.3	0.4	13.0	9.2	1.0
A2	0.04	0.32	3.9	1.0	24.3	15.1	–

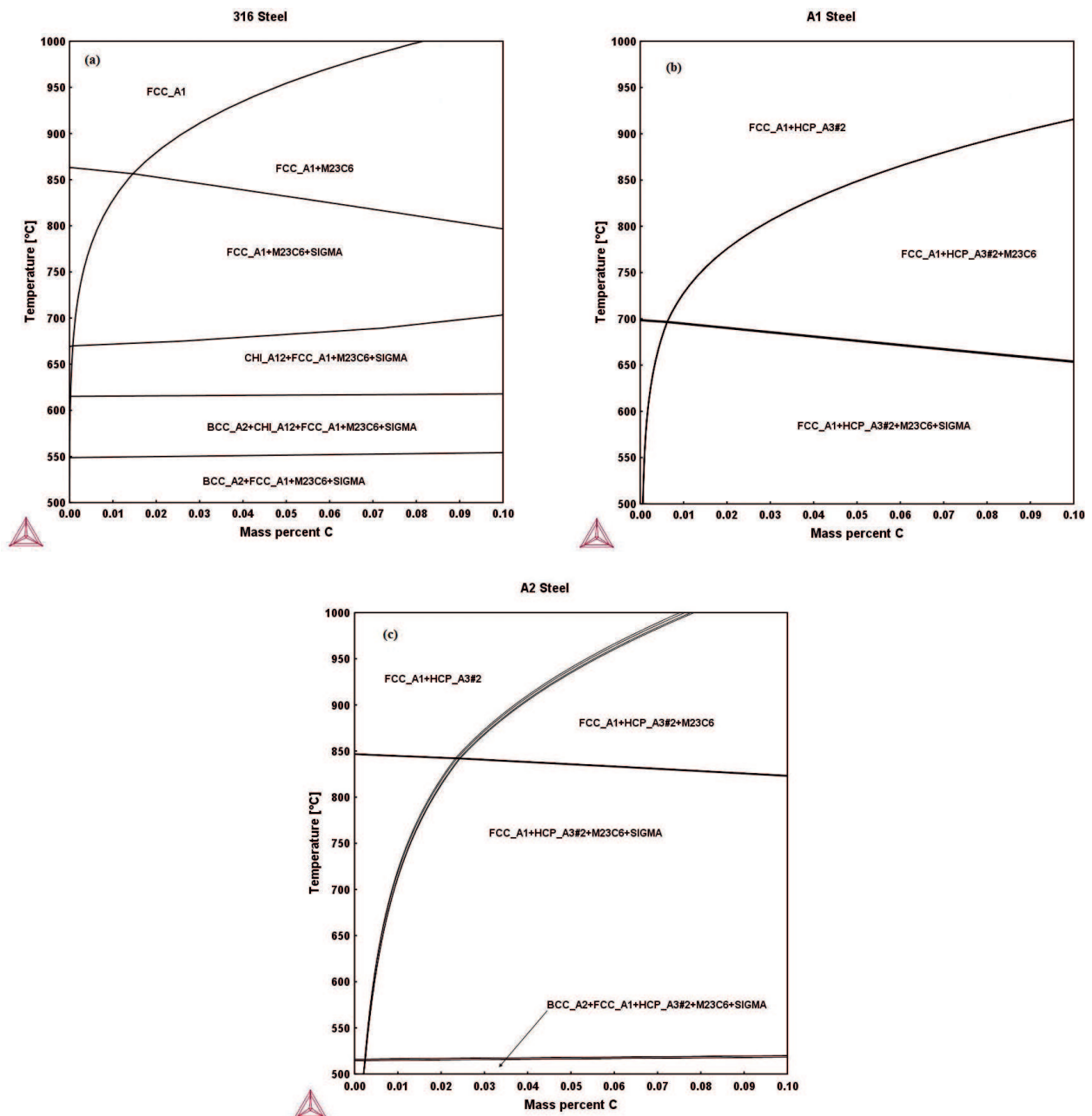**Table 1.** Chemical composition of steels in wt.%.

Figure 1. Equilibrium pseudobinary Fe-C phase diagrams for (a) 316, (b) A1, and (c) A2 steels.

1000 min. The TTP diagram for 316 steel is shown in **Figure 3(a)** and it can be noticed that the following precipitation reaction takes place:

$$\gamma_{sss} \ \rightarrow \ \gamma + M_{23}C_6 \qquad\qquad (1)$$

The fastest growth kinetics of precipitation is at a temperature slightly lower than 700°C. Besides, no σ phase is formed at these temperatures for short aging times. This fact is in good agreement with the experimental TTP diagrams reported in the literature [1].
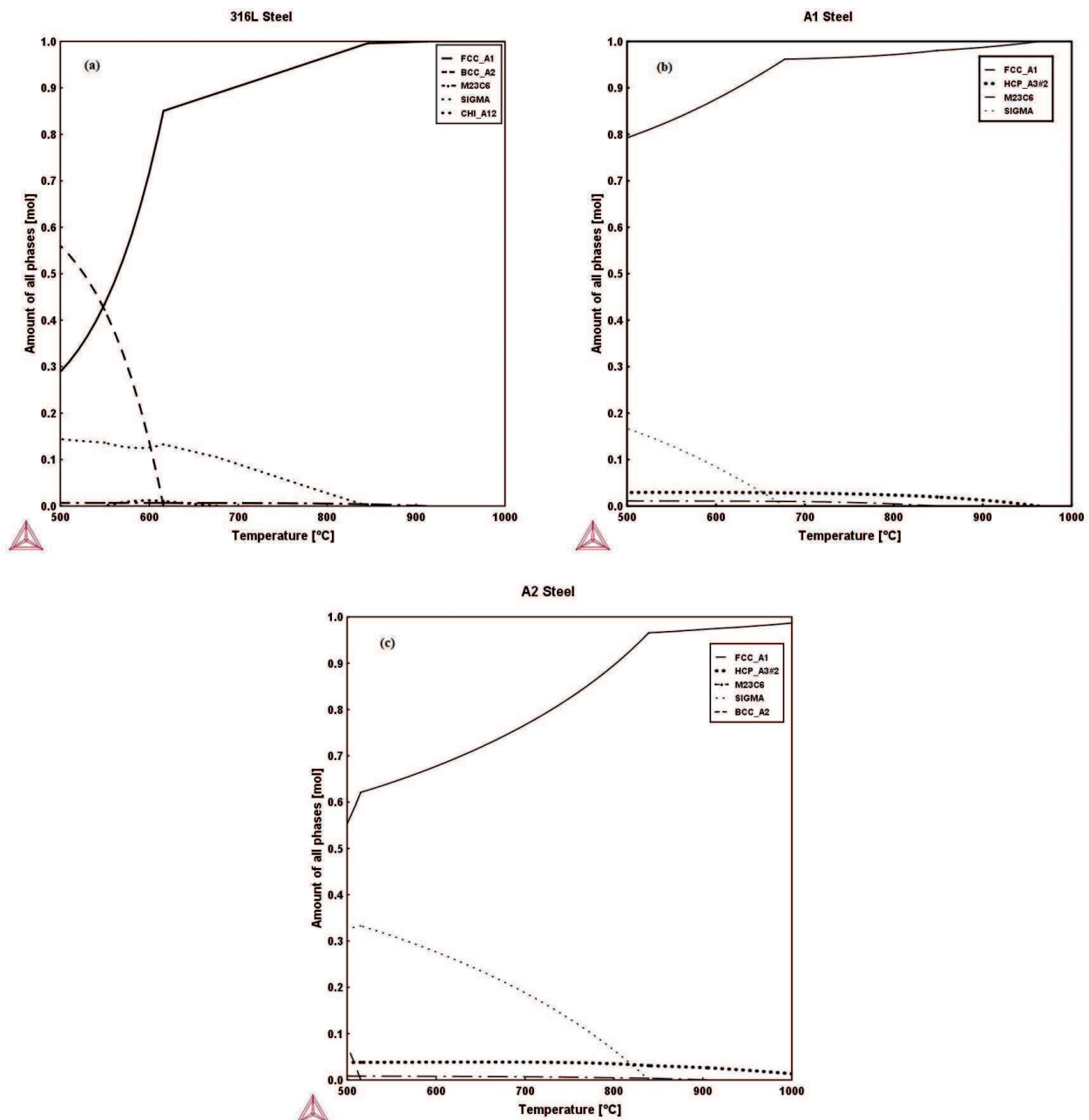
Figure 2. Amount of all phase vs. temperature for (a) 316, (b) A1, and (c) A2 steels.

In the case of both N-containing A1 and A2 steels, the following precipitation reaction is observed to occur in the TTP diagrams, **Figure 3(b, c)**:

$$\gamma_{sss} \rightarrow \gamma + M_2N \qquad (2)$$

That is, the aging at these temperatures for times up to 1000 min only promotes the precipitation of nitrides. The growth kinetics of precipitation occurs more rapidly in the
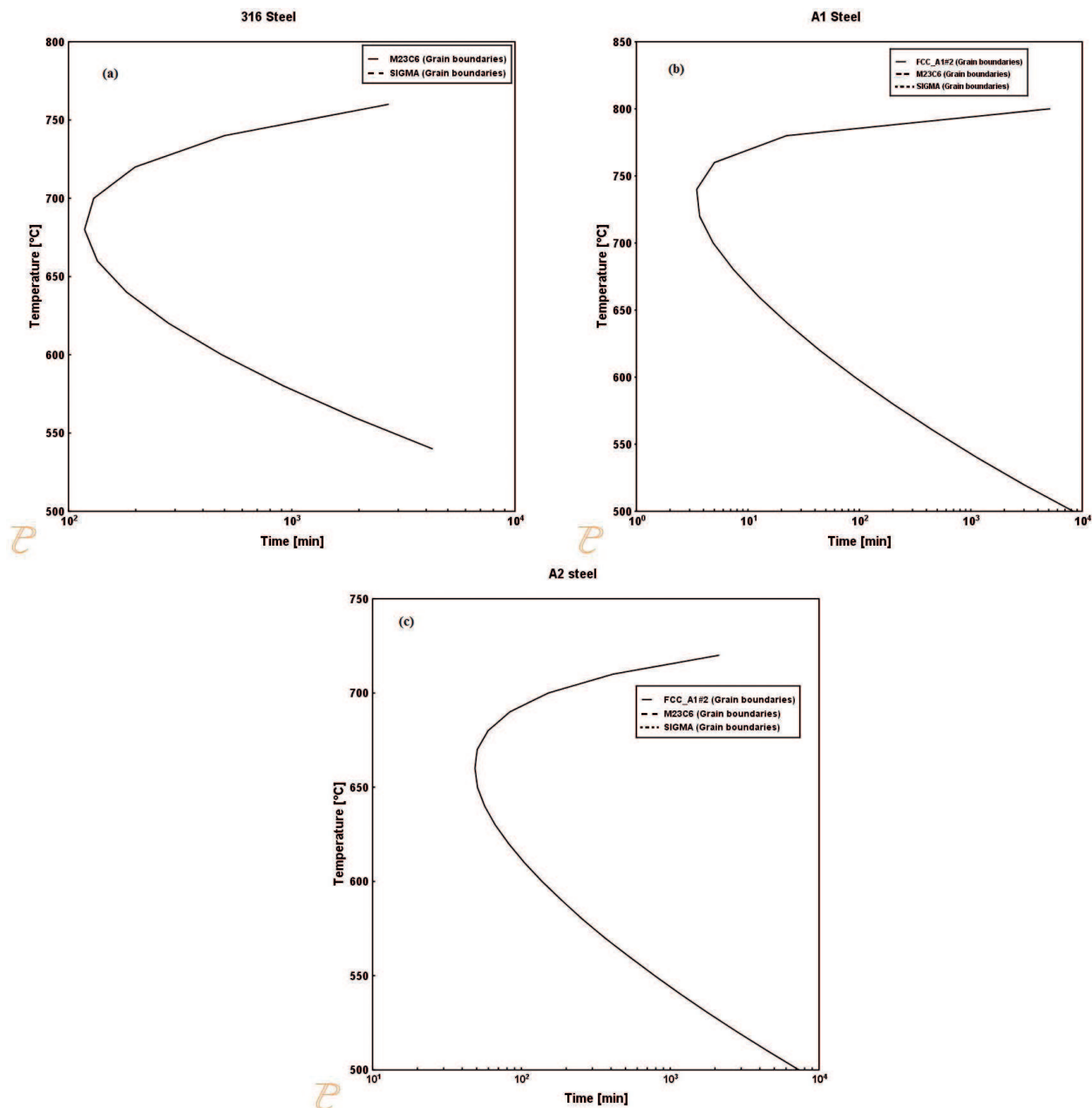
Figure 3. TTP diagram for (a) 316, (b) A1, and (c) A2 steels.

316 steel than that of A1 and A2 steels, which can be attributed to the lower content of interstitial solute causing a faster atomic diffusion process [2, 9]. The same reason can be adopted to explain the faster growth kinetics for aging of A1 steel. No σ phase and $M_{23}C_6$ formation is observed for these aging conditions. This behavior is in agreement with results reported in the literature [10, 11]. These diagrams show that the aging time for the intergranular carbide or nitride precipitation is very short; thus, this may be expected during the cooling at temperatures between 600 and 900°C in the welding process of the materials.

3. Microstructure evolution during aging

The SEM microstructures of the as-received 316, A1, and A2 steels are shown in **Figure 4(a–c)**, respectively. An austenite matrix is clearly observed for all the cases. Besides, neither intra-granular nor intergranular precipitation is observed for this condition.
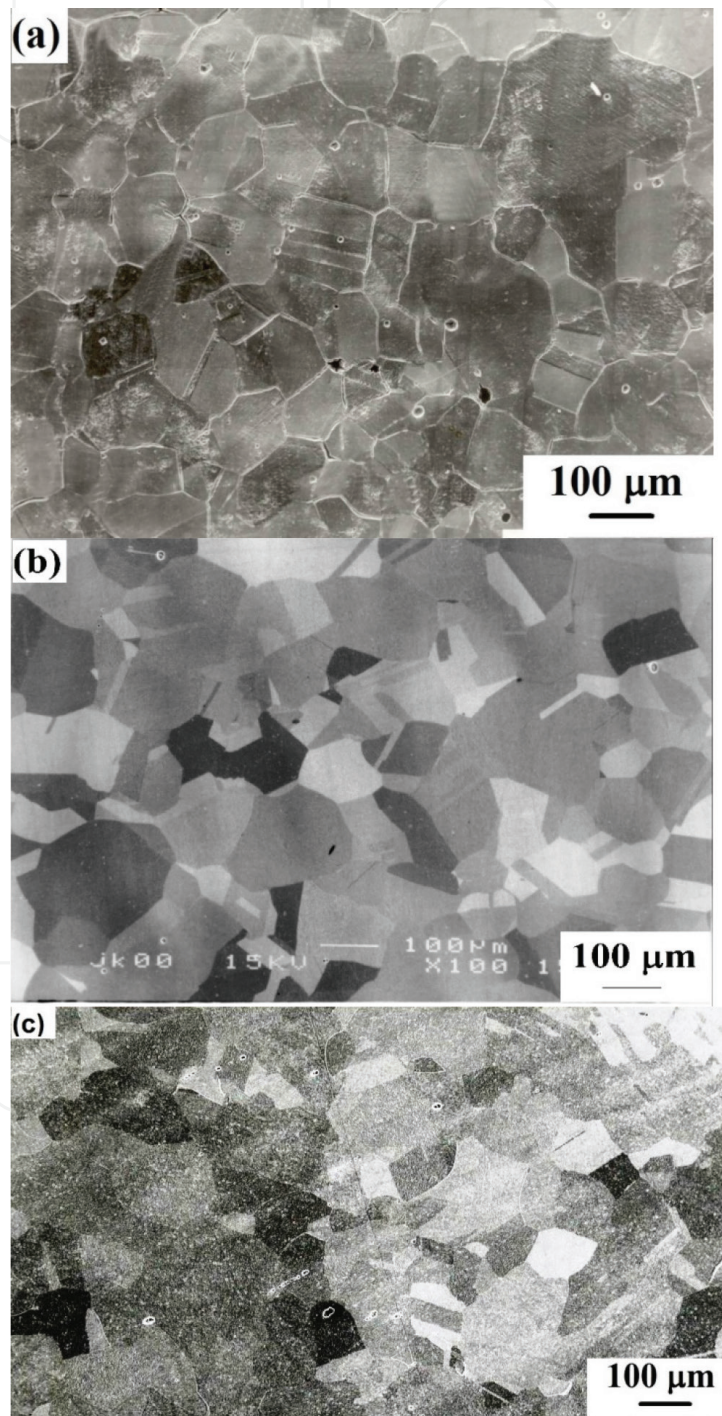

Figure 4. SEM micrographs of as-received (a) 316, (b) A1, and (c) A2 steels.

Figure 5(a–f) illustrates, for instance, the SEM micrograph for 316, A1, and A2 steels after aging at 700°C for 10 and 1000 min, respectively. An intergranular precipitation can be observed on the austenite grain boundaries for all cases. The presence of intergranular precipitation is in good agreement with all the TTP diagrams. The highest and lowest volume fractions of intergranular precipitation correspond to the A2 and 316 steels, respectively. This is attributable to the highest content of interstitial solutes for the former steel. Conversely, the 316 steel has the lowest content of interstitial solutes. The volume fraction increases, in general with aging time. Nevertheless, the calculated growth kinetics is not in good agreement with the experimental precipitation observed in both the aged A1 and A2 steels, since the intergranular precipitation is present for aging times as short as 10 min. This fact can be attributed to the values of interfacial energy utilized in the TC-PRISMA calculation. In the case of 316 steel, the precipitation presence in observed at temperatures as high at 900°C for aging times up to 1000 min; however, the corresponding TC-PRISMA-calculated TTP diagram that shows a very slow kinetics of precipitation at 900°C.
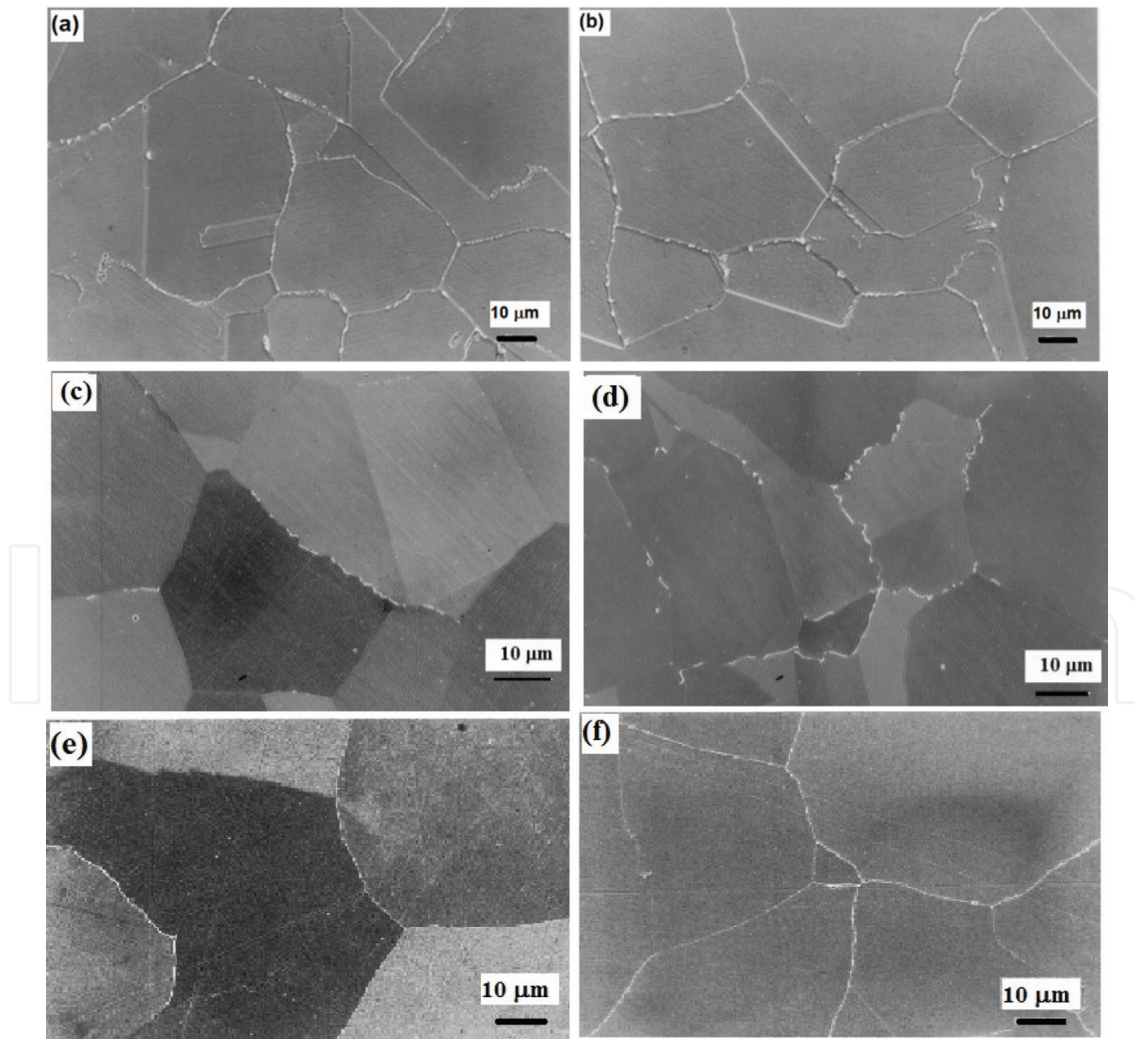

Figure 5. SEM micrographs of (a, b) 316, (c, d) A1, and (e, f) A2 steels aged at 700°C for 10 and 1000 min, respectively.

The XRD patterns of precipitates, extracted from electrolytic dissolution of the austenite matrix, are shown in **Figure 6(a, b)** for the 316 and A1 steels, respectively, aged at 700°C for 1000 min. These indicate that the precipitated phases correspond to $Cr_{23}C_6$, and $Cr_{23}C_6$ and Cr_2N for the aged 316 and A1 steels, respectively. The presence of $Cr_{23}C_6$ carbide is in good agreement with the TC-PRISMA-calculated TTP diagram for 316 steel; however, the N-containing steel shows the existence of both $Cr_{23}C_6$ and Cr_2N phases, which is not observed in the TC-PRISMA-calculated TTP diagram for the A1 steel. This can be also attributed to the interfacial energy between austenite matrix and carbide used for the TTP calculation. The nitrides and carbides detected in the XRD patterns are not only composed of Cr,
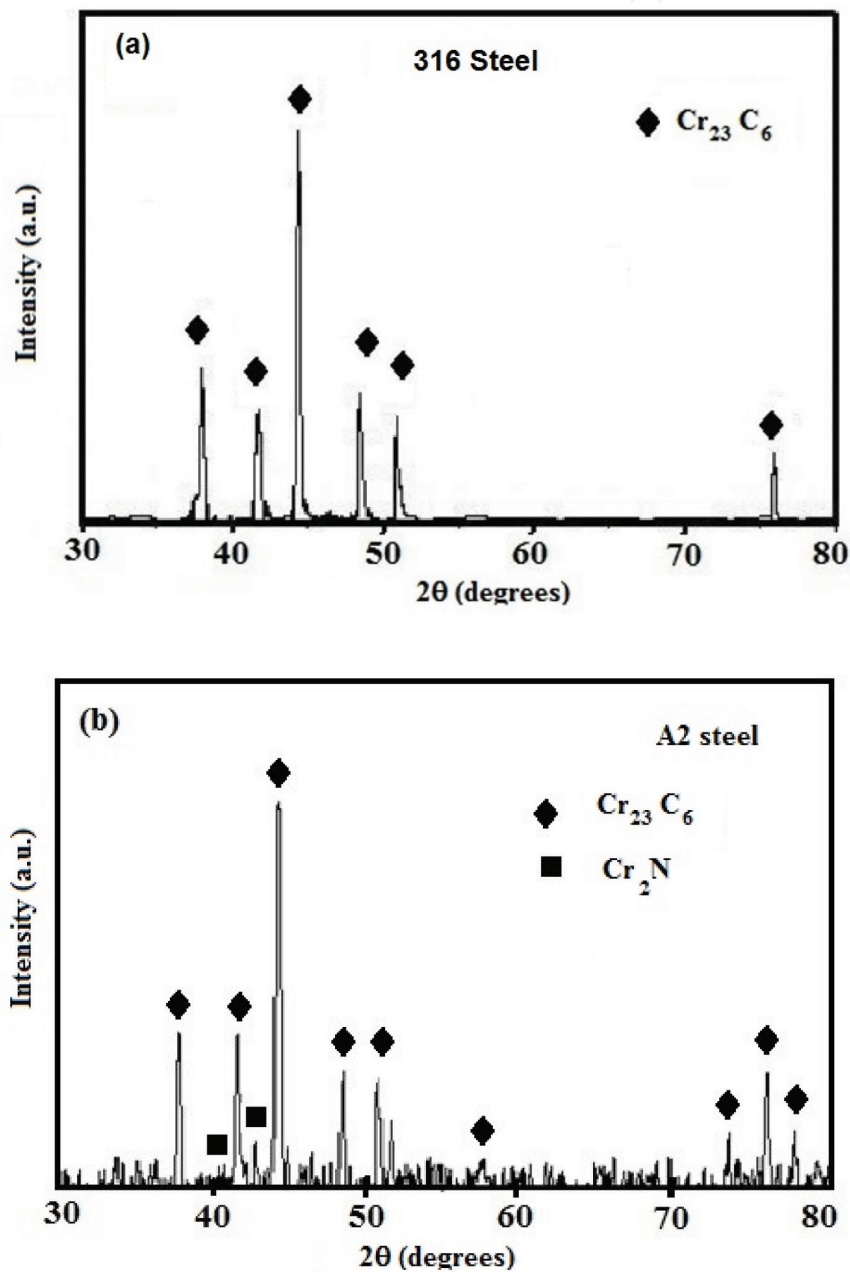

Figure 6. XRD pattern of (a) 316 steel and (b) A1 steel aged at 700°C for 1000 min.

but these are also formed by Fe and Mo according to the EDX-SEM analysis and composi-tions calculated by Thermo-Calc. Thus, they are designated as $M_{23}C_6$ and M_2N.

The experimental TTP diagrams, determined by SEM observations, for the three steels are shown in **Figure 7(a–c)**. The TTP corresponding to the 316 steel shows the intergranular pre-cipitation of $M_{23}C_6$ carbides for all aging temperatures and times, **Figure 7(a)**, which is in good
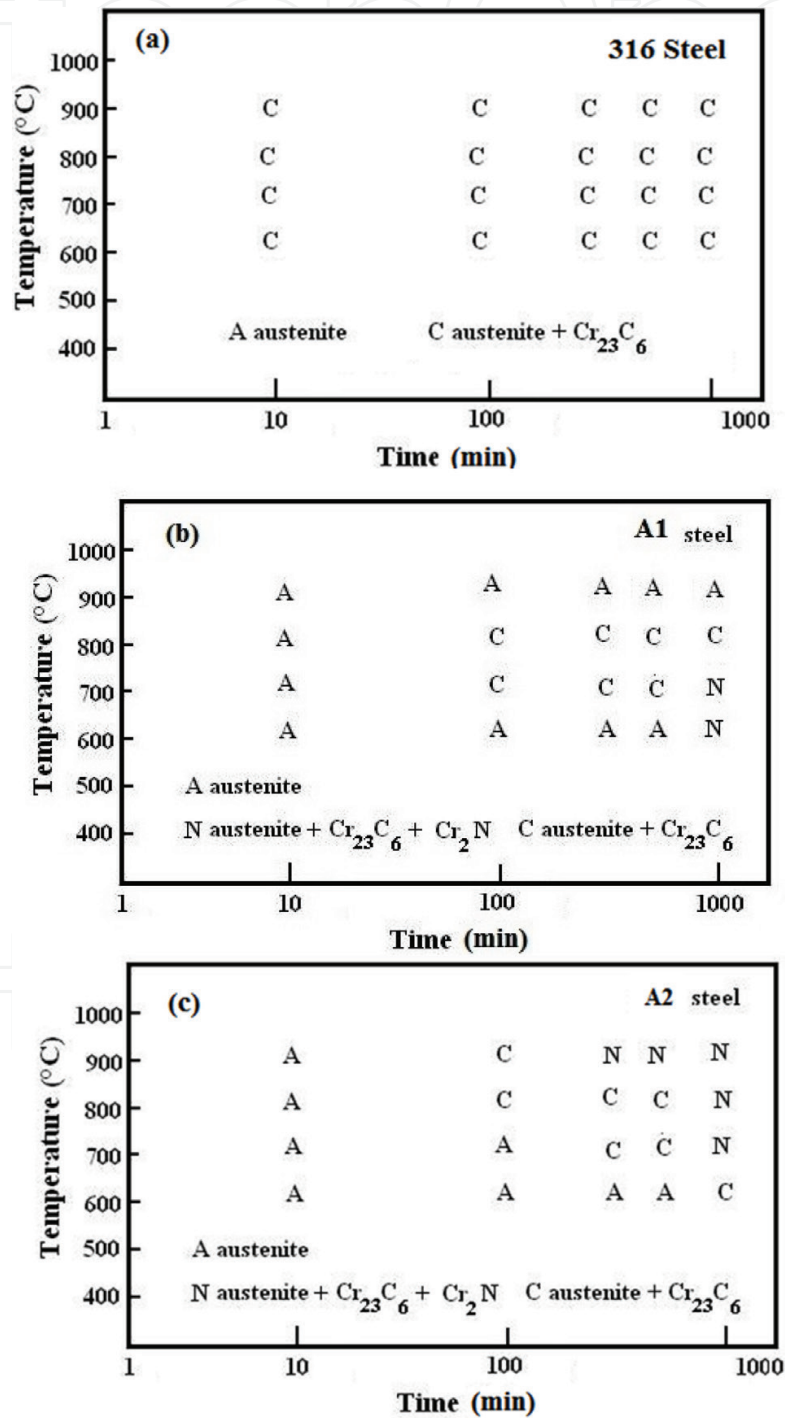

Figure 7. Experimental TTP diagram for (a) 316, (b) A1, and (c) A2 steels.

agreement with the calculated TTP diagram of 316 steel. That is, the growth kinetics of carbide is fast for all temperatures. The growth kinetics of carbide precipitation increases with aging temperature.

Figure 7(b) shows the experimental TTP for the A1 steel. This indicates that there is almost no precipitation at 600 and 900°C. The calculated TTP diagram for this steel, **Figure 3(b)**, exhibits no precipitation at 900°C, but there is nitride precipitation at aging temperature of 600°C. As mentioned above, this disagreement can be attributed to the values of interfacial energy between matrix and precipitate used for the TC-PRISMA calculation. In contrast, the experimental TTP diagram of the A2 steel, **Figure 7(c)**, presents precipitation at all temperatures being the slowest kinetics at 600°C, which agrees with the calculated TTP diagram, **Figure 3(c)**. It is important to note that the aging times for intergranular precipitation are very short at temperatures of 600–900°C; thus, the intergranular precipitation may be expected to occur during the welding process of thick structural sections. This fact may involve problems of sensitization or thermal aging.

4. Effect of precipitation on cryogenic toughness

Plots of CVN impact test energy at −196°C as a function of aging time for the three steel aged at different temperatures are shown in **Figure 8(a–c)**. In general, the impact energy decreases with aging time as a result of the increase in volume fraction of intergranular precipitates. In the case of the aged 316 steel, there is almost no decrease in impact energy for the specimens aged at 600 and 700°C, which is consistent with the low volume fraction of carbides detected at these temperatures. The highest decrease takes place for the specimen aged at 900°C, which observed the occurrence of the fastest growth kinetics of precipitation; and thus, the highest volume fraction of precipitates.

In the case of N-containing steels, the highest decrease in impact energy occurs at aging temperatures of 800 and 900°C for the A1 and A2 steels, respectively. The fastest growth of kinetics of precipitation was also observed to take place at those temperatures. No decrease in energy was observed practically to occur for aging of A1 steel at 900°C. In contrast, the decrease in energy was more drastic for aging of A2 steel as the aging time and temperature increase. This is attributable to the highest volume fraction of intergranular nitrides observed at this aging condition.

The SEM fractographs of CVN impact test specimens are shown in **Figure 9(a–f)** for the 316, A1, and A2 steel aged at 700°C for 0 (as-received) and 1000 min, respectively. The fracture mode was transgranular ductile, **Figure 9(a, b)**, for both the as-received and aged 316 steel specimens. This behavior suggests that the intergranular precipitation has a small effect on the toughness at cryogenic temperature. In contrast, the fracture mode of the aged A1 and A2 steels changes from transgranular ductile to intergranular brittle as the aging time increases, **Figure 9(c–f)**. The presence of intergranular brittle fracture can be more clearly noted in the aged A2 steels. This change in fracture mode can be attributed to the intergranular precipitation of nitrides.
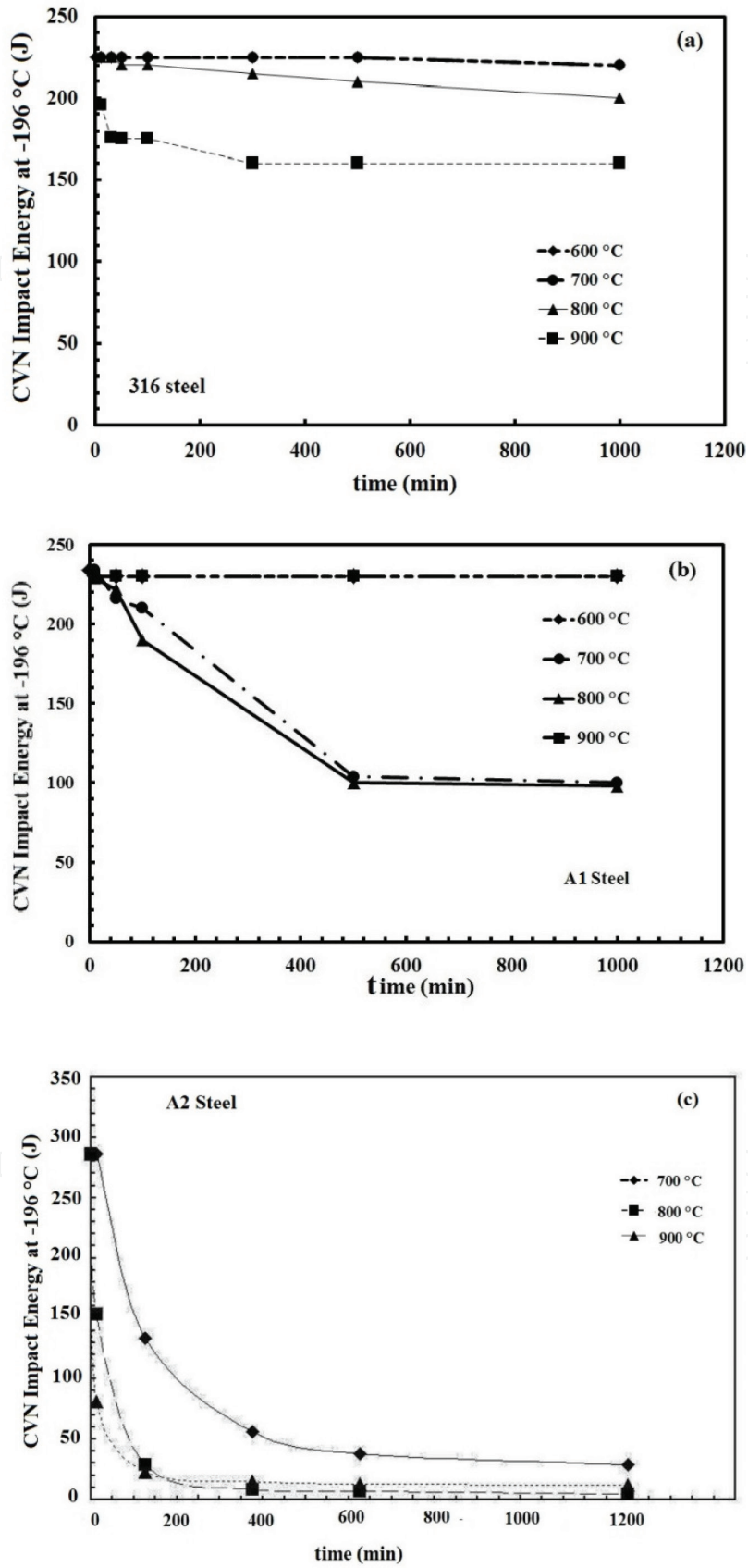
Figure 8. CVN impact energy at −196°C for the aged (a) 316, (b) A1, and (c) A2 steels.
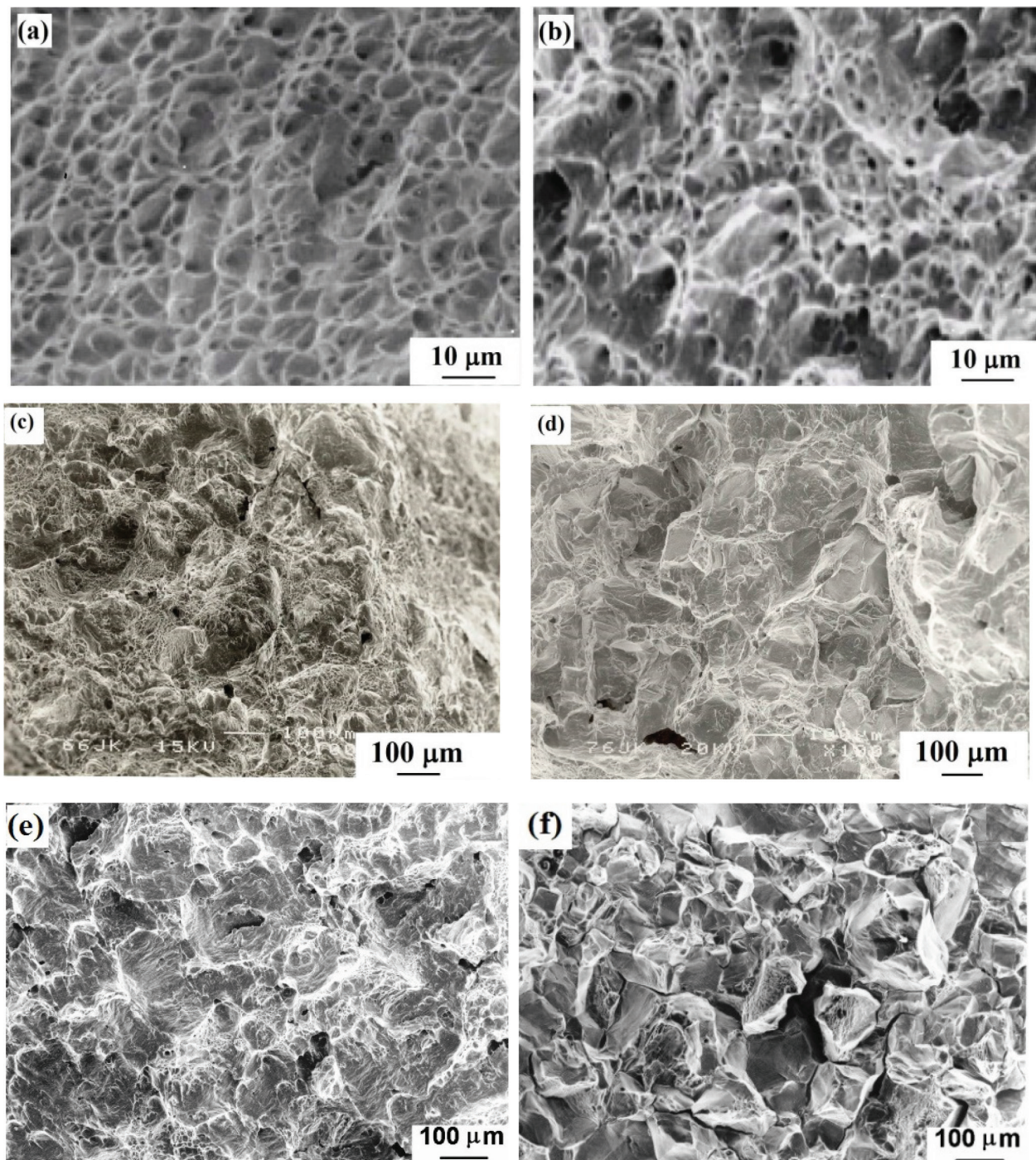
Figure 9. SEM fractographs of CVN impact specimens at −196°C for the (a, b) 316, (c, d) A1, and (e, f) A2 steels aged at 700°C for 0 and 1000 min, respectively.

The variation of CVN impact test energy at −196°C with the volume fraction of intergranular precipitates is shown in **Figure 10** for the aged A1 and A2 steels. These figures show clearly that the impact energy decreases with the increase in volume fraction of intergranular precipitates promoting the intergranular brittle fracture. This fact suggests that the intergranular precipitates cause the loss of cohesion of grain boundaries, as shown in **Figure 11**. This figure shows precipitate chains on grain boundaries for the A2 steel aged at 900°C for 10 min.
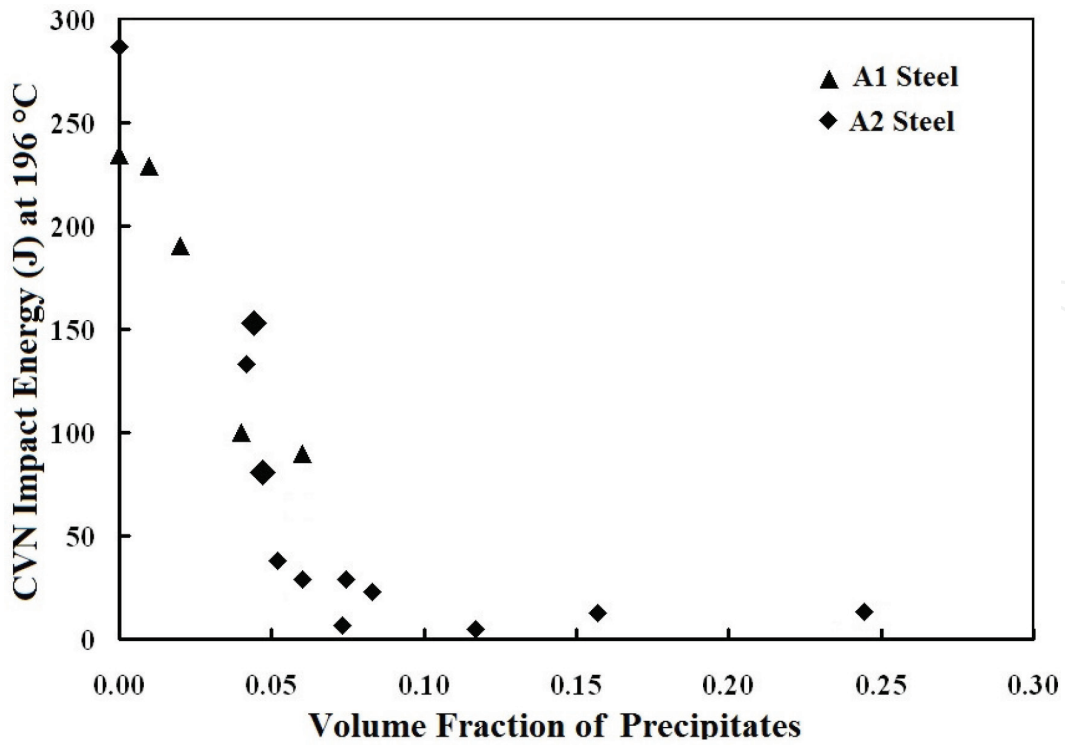
Figure 10. Plot of CVN impact test energy vs. volume fraction of precipitates for N-containing steels.
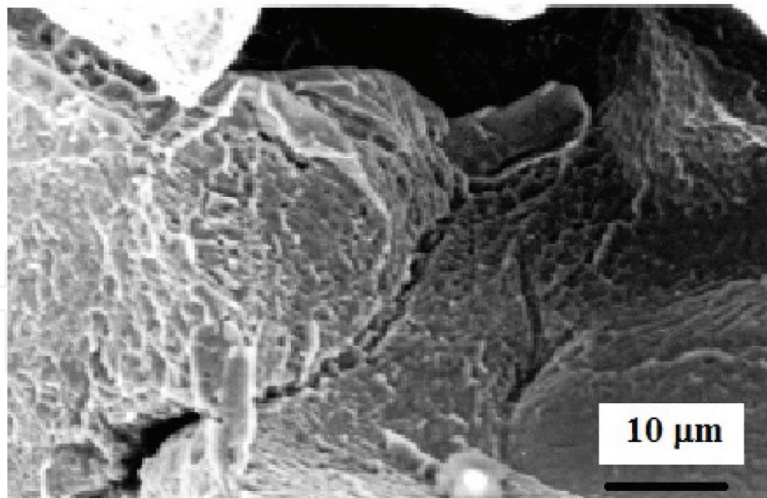
N-containing steels

Figure 11. SEM fractograph of CVN impact test specimen of A2 steel aged at 900°C for 1000 min.

It is important to point out that the N-containing A1 and A2 steels have higher mechanical properties at cryogenic temperatures than those of the 316 steel; however, the former steels are more susceptible to the grain boundary embrittlement.

5. Summary

This chapter shows the effect of precipitation on cryogenic toughness for N-containing steels. The presence of intergranular nitride precipitates causes a severe decrease in CVN impact test energy for steels after aging at temperatures between 700 and 900°C for times as short as 10 min. This fact is attributable to its higher volume fraction of intergranular nitride precipitates due to their higher interstitial solute contents in comparison to 316-type steels. In contrast, the 316 steel shows a better resistant to the decrease in impact energy after aging in spite of the faster growth kinetics of precipitation. N-containing steels exhibit the presence of intergranular brittle fracture as a result of the grain boundary nitride precipitation. This behavior may be also present during the welding of this type of nitrogen-containing steels because of the short aging time for precipitation.

Acknowledgements

Author details

Maribel L. Saucedo-Muñoz* and Victor M. Lopez-Hirata

*Address all correspondence to: maribelsaucedo@prodigy.net.mx

Instituto Politecnico Nacional (ESIQIE), CDMX, Mexico

References

[1] Marshall P. Austenitic Stainless Steels. 1st ed. London: Elsevier; 1984. 50 p

[2] Gavriluj VG, Berns H. High Nitrogen Steels. Berlin: Springer; 1999. 20 p

[3] Simmons JW, Atteridge DG, Rawers JC. Sensitization of high-nitrogen austenitic stainless steels. Corrosion. 1994;**50**:491-501. DOI: https://doi.org/10.5006/1.3294349

[4] Sedrinks AJ. Corrosion of Stainless Steels. 1st ed. New York: John Wiley and Sons Inc.; 1996. 13 p

[5] Stoter LP. Thermal ageing effects in AISI type 316 austenitic stainless steel. Journal of Materials Science. 1981;**16**:1039-1051. DOI: 10.1007/BF00542750

[6] Thermo-Calc. Thermo-Calc Software [Internet]. 2017. Available from:http://www.thermocalc.com/pro ducts-services/software/thermo-calc/ [Accessed: 2017-07-11]

[7]   Thermo-Calc. Precipitation Module TC-PRISMA [internet]. 2017. Available from:http://www.thermocalc.com/products-services/software/precipitationmodule-(tc-prisma)/ [Accessed: 2017-07-11]

[8]   Pettersson N., Frisk K., Fluch R. Experimental and computational study of nitride precipitation in a CrMnN austenitic stainless steel. Mat. Sci. Eng. A. 2017;**684**:435-441. DOI: http://dx.doi.org/10.1016/j.msea.2016.12.071

[9]   Kostorz G. Phase Transformations in Materials. New York: Springer; 2001. 309 p.

[10]   Saucedo-Muñoz ML, Watanabe Y, Shoji T, Takahashi H. Effect of microstructure evolution on fracture toughness in isothermally aged austenitic stainless steels for cryogenic application. Cryogenics. 2000;**40**:693-700. DOI: https://doi.org/10.1016/S0011-2275(01)00004-2

[11]   Saucedo-Muñoz ML, Liu CS, Komazaki S, Kwon I, Hashida T, Takahashi H, Nakajima H. Evaluation of thermal aging embrittlement of austenitic stainless steels JN1, JJ1 and JK2 by cryogenic small-punch testing. Journal of Materials Research. 2002;**17**:852-858. DOI: http://dx.doi.org/10.1557/JMR.2002.0124